Commun. Comput. Phys.
doi: 10.4208/cicp.060414.220115a

Vol. **18**, No. 2, pp. 489-515
August 2015

Immersed Boundary – Thermal Lattice Boltzmann Methods for Non-Newtonian Flows Over a Heated Cylinder: A Comparative Study

A. Amiri Delouei[1], M. Nazari[1,*], M. H. Kayhani[1] and S. Succi[2]

[1] *Department of Mechanical Engineering, University of Shahrood, Shahrood, Iran.*
[2] *IAC-CNR, Rome, Via dei Taurini 19, 00185, Roma & Department of Physics, Harvard University, Oxford Street 60, Cambridge, MA 02138, USA.*

Communicated by Boo-Cheong Khoo

Received 6 April 2014; Accepted (in revised version) 22 January 2015

Abstract. In this study, we compare different diffuse and sharp interface schemes of direct-forcing immersed boundary — thermal lattice Boltzmann method (IB-TLBM) for non-Newtonian flow over a heated circular cylinder. Both effects of the discrete lattice and the body force on the momentum and energy equations are considered, by applying the split-forcing Lattice Boltzmann equations. A new technique based on predetermined parameters of direct forcing IB-TLBM is presented for computing the Nusselt number. The study covers both steady and unsteady regimes ($20<Re<80$) in the power-law index range of $0.6< n <1.4$, encompassing both shear-thinning and shear-thickening non-Newtonian fluids. The numerical scheme, hydrodynamic approach and thermal parameters of different interface schemes are compared in both steady and unsteady cases. It is found that the sharp interface scheme is a suitable and possibly competitive method for thermal-IBM in terms of accuracy and computational cost.

AMS subject classifications: 65Y20, 76A05, 76D25, 76P05, 76R05

Key words: Immersed Boundary Method, Thermal Lattice Boltzmann Method, non-Newtonian fluid, cylinder, power-law fluids.

1 Introduction

The problem of Newtonian fluid flow and heat transfer over a cylinder has been studied by several researchers as a benchmark for verification of solution methods in complicated geometries [1–3]. This flow configuration provides valuable insights into the

*Corresponding author. *Email addresses:* a.a.delouei@gmail.com (A. A. Delouei), mnazari@shahroodut.ac.ir (M. Nazari), h_kayhani@shahroodut.ac.ir (M. H. Kayhani), s.succi@iac.cnr.it (S. Succi)

 ©2015 Global-Science Press

https://doi.org/10.4208/cicp.060414.220115a Published online by Cambridge University Press

nature of the fundamental physical interaction phenomena involving momentum and heat transfer, [4]. Due to the abundance of industrial applications, such as the formation of weld lines in polymer processing operations [5], the use of thin cylinders and wires as measurement probes and sensors in non-Newtonian flows [6], in the resin transfer molding process of manufacturing fiber reinforced composites [6], thermal treatment of various food-stuffs [4], fluidized bed drying of fibrous substances [4], non-Newtonian fluids flows have entered into this discussion. In comparison with the work developed in the field of non-Newtonian fluids flow in presence of immersed body [7], the thermal investigation of these fluids is less extended, even for the flow of Newtonian fluids over a heated circular cylinder [8]. In fact, the few studies in this area have employed finite volume methods using FLUENT software [8–10] or finite difference methods [11].

Recently, some progress, based on the immersed boundary idea of Peskin [12], has been accomplished, which can simplify the solution in complex geometries. The immersed boundary method (IBM) was first proposed by Peskin [12] to investigate flow patterns around heart valves, without any body-fitted mesh. Over the years, the IBMs have been improved and overcome most of the original limitations of original Peskin method [13, 14]. At present, the IBM has gained a prominent role for the numerical simulation of complex fluid-structure interactions [15]. The IBM can be categorized both as a mathematical formulation and as a numerical scheme. A combination of Eulerian and Lagrangian variables are considered in the mathematical formulation. An interaction equation linked these two types of variables. In the numerical aspect of IBM, the Eulerian variables are denoted by fixed Cartesian mesh while, the Lagrangian variables are traced via a completely separated curvilinear mesh, with the ability of moving freely across the fixed Eulerian nodes (see Fig. 1). Generally speaking, the IBM is a non-body-conformal grid method that satisfies the no-slip boundary condition (or thermal boundary condition) by implementing a force density (or an energy-force density) term within the flow governing equation (or the energy equation). With respect to the algorithm of the boundary force evaluation, at least three general groups of IB methods can be identified: (i) feedback-forcing method, (ii) direct-forcing method, and (iii) momentum exchange-based method. The former employs the feed-back process based on the position (and/or velocity, temperature) of the boundary points [12] and the second one utilizes the flow equation (or energy equation) to regulate the boundary force (or boundary energy-force) density [17]. In the third group (for example [18, 19]), the forcing term is computed via the momentum exchange method introduced by Ladd [20].

The dependency of two non-coincident Eulerian and Lagrangian grids can be established by interface schemes based on a smoothed approximation of the Dirac delta function (diffuse interface scheme) [21] or a sharp interpolations (sharp interface schemes) [22]. The choice of the appropriate interface scheme is another very important issue beside the force evaluation method in the IBM [23]. We shall present detailed comparisons in the following.

As mentioned above, in the IBM, the Eulerian grids should be placed in a Cartesian frame; the Lattice Boltzmann Method (LBM) is an excellent solver which satisfies this

https://doi.org/10.4208/cicp.060414.220115a Published online by Cambridge University Press

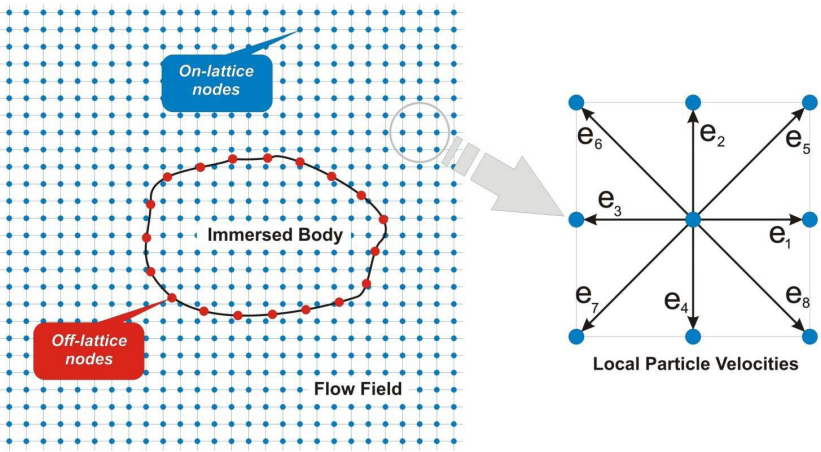


Figure 1: Schematic of an immersed body in the fluid field and lattice velocity direction [16].

requirement. In addition, the LBM has the advantages of simplicity, computational efficiency and parallel scalability, high resolution and kinetic theory basis [24], which points to it as a preferred choice for denoting the Eulerian mesh grid in the current study. The limitations of the LBM for simulating of Newtonian flows have improved significantly in recent years [25–29]. Unlike to the Newtonian fluids, the viscosity of non-Newtonian fluids is a non-linear function of shear rate. The non-constant viscosity of non-Newtonian fluids can leads to some instabilities in the simulation process [30]. However, as an another advantage of LBM with respect to ordinary CFD methods in the case of non-Newtonian fluid, the LBM have ability of straightforward calculations of the local shear rate to second-order accuracy independent of the velocity field. This advantage comes from the kinetic nature of LBM [31]. In the moderate Reynolds number which is interested here, most of the researchers employ the non-Newtonian power-Law model for investigating the shear-thinning and shear-thickening fluids. This model can effectively capture the non-Newtonian behavior of shear-thinning and shear-thickening fluids in the range of Reynolds number interested here.

Although the several modified LBMs are existed for simulations of fluid flows in geometries which include curved boundaries [32,33], but due to uniform Cartesian lattices, the implementation of LBM for curved boundaries requires rather lengthy calculation and procedures. Unlike the modified LBM, in the immersed boundary-lattice Boltzmann method (IB-LBM), the Eulerian nodes are completely solved in a fixed Cartesian grid independent on the shape and movement of immersed body. In other words, the IB-LBM merges the best properties of both immersed Boundary and lattice Boltzmann methods. Cheng et al. [34] studied the numerical stability and accuracy of IB-LBM. The immersed boundary - thermal lattice Boltzmann method (IB-TLBM) is also extended to the energy equation by some researchers. Kang and Hassan [23, 35] used IB-LBM and IB-TLBM for simulation of fluid flow in isothermal and non-isothermal Newtonian flows, respectively.

https://doi.org/10.4208/cicp.060414.220115a Published online by Cambridge University Press

They claim that the sharper interface schemes have more accurate results for stationary Newtonian flows. Amiri Delouei et al. [16] studies non-Newtonian thermal flows over circular cylinder by using diffuse interface schemes. Also, Fu et al. [36, 37] used the IB-LBM to model blood flow in constricted pipes. They reported both Newtonian and non-Newtonian flows in their studies. Wu and Shu [38, 39] proposed a new boundary condition-enforced IB-LBM for studying the fluid-solid interactions in Newtonian fluids. In these works, the force is determined by the no-slip boundary condition, and flow penetrations occur in the feed-back forcing procedure and direct-forcing methods is avoided. Regarding to their researches, when this kind of diffuse interface IBM is combined with LBM, it would perform as well as the sharp interface IBM. Their boundary condition-enforced IBM was developed to thermal flows by Wu et al. [40], Shu et al. [41], and Ren et al. [42, 43].

This paper is concerned primarily with the task of developing and comparing of direct-forcing IB-TLBM with different interface schemes for shear-thinning and shear thickening non-Newtonian fluids. Regarding the available results, the benchmark problem of unconfined fluid flow and heat transfer over a stationary heated cylinder is chosen. In order to consider both discrete lattice effect and influence of the body force on the momentum and energy equations, the split-forcing lattice Boltzmann method proposed by Guo et al. [44] has been employed. This method can recover the Navier-Stokes equations exactly [44] and introduced as the preferred method by several researchers [23, 44]. Similar to the force evaluation method, the interface scheme directly influences the accuracy of the IBM and the appropriate selection of the interface scheme has an important role in the precision of the IB-TLBM. Here, for the first time, the most common interface schemes consist of 2-points [23], 3-points [45], 4-points [15] and cosine-type of 4-points [46] diffuse and sharp interface schemes of IB-TLBM are adopted and compared for the case of non-Newtonian flow subjected to the heated cylinder. Also, a new simple technique for computing the Nusselt number in steady and unsteady flows based on the predetermined parameters of direct forcing IB-TLBM is developed, which helps reducing the computational complexity and computational cost of the process.

The structure of the paper is as follows: the numerical procedures of the proposed direct-forcing IB-TLBM are discussed in Section 2. In Section 3, the different interface schemes which are utilized for the current investigation is explained in details. It must be noted that because of stationary condition of cylinder, the Eulerian and Lagrangian mesh grids are denoted by 'on-lattice' and 'off-lattice' nodes, respectively. The relevant dimensionless parameters here are defined and the methods of assessment of them in IB-TLBM are described in Section 4. In Section 5, the verification of proposed solution is presented. Also the comparison study for different interface schemes of IB-TLBM is done in three aspects including (i) the numerical scheme, (ii) hydrodynamic approach and (iii) thermal parameters both in steady and unsteady cases. It is found that the prediction of hydrodynamic phenomena associated with this configuration is more accurate by sharp interface scheme in steady flow regimes especially, for shear-thinning non-Newtonian fluid flows.

https://doi.org/10.4208/cicp.060414.220115a Published online by Cambridge University Press

2 Immersed boundary – thermal lattice Boltzmann method for non-Newtonian flow

In this section, the numerical methods applied for the current study are discussed. Here direct-forcing IB-TLBM is used for both velocity and temperature fields. Also, the split-forcing LBE is utilized for more effective evaluation of boundary force density. The non-Newtonian lattice Boltzmann formulations is introduced in details.

2.1 The split-forcing thermal LBE

The double population approach is used as the thermal model in the current study. In the double population model, the governing equations can be separated as the density distribution f_i and the internal energy density distribution g_i to investigate the flow and temperature fields, respectively. The single relaxation time LBE with an unsteady, non-uniform, body-force density term for the fluid flow (in space $\vec{x}$ and time t) can be expressed as follows [23]:

$$f_i(\vec{x}+\vec{e}_i\Delta t,t+\Delta t)=f_i(\vec{x},t)-\frac{1}{\tau_f}\left[f_i(\vec{x},t)-f_i^{(eq)}(\vec{x},t)\right]+F_i(\vec{x},t)\Delta t, \tag{2.1}$$

and the simplified Thermal LBE with an energy source can be written as [35]

$$g_i(\vec{x}+\vec{e}_i\Delta t,t+\Delta t)=g_i(\vec{x},t)-\frac{1}{\tau_g}\left[g_i(\vec{x},t)-g_i^{(eq)}(\vec{x},t)\right]+Q_i(\vec{x},t)\Delta t, \tag{2.2}$$

where $\vec{e}_i$ is the particle velocity vector in the i^{th} velocity direction of the lattice. $f_i(\vec{x},t)$ and $g_i(\vec{x},t)$ are the particle density and internal energy density distribution functions of the i^{th} direction, respectively. Also, $F_i(\vec{x},t)$ and $Q_i(\vec{x},t)$ are the discrete external force and discrete energy source functions of the i^{th} direction, respectively. τ_f and τ_g are the single relaxation times related to the fluid flow and energy equations, respectively. The single relaxation times control the rate of approach from the non-equilibrium state to the equilibrium state. Here, the two-dimensional nine-velocity (D2Q9) model is used which is (refer to Fig. 1):

$$\vec{e}_i=c\begin{bmatrix}1&0&-1&0&1&-1&-1&1&0\\0&1&0&-1&1&1&-1&-1&0\end{bmatrix}, \tag{2.3}$$

where $c=\Delta x/\Delta t$ is the lattice speed. Δx and Δt are the lattice size and the time step size, respectively. The equilibrium distribution function, $f_i^{(eq)}(\vec{x},t)$, and the equilibrium

https://doi.org/10.4208/cicp.060414.220115a Published online by Cambridge University Press

internal energy density distribution function, $g_i^{(eq)}(\vec{x},t)$, can be introduced as:

$$f_i^{(eq)} = w_i\rho\left[1+\frac{3}{c^2}(\vec{e}_i\vec{u})+\frac{9}{2c^4}(\vec{e}_i\vec{u})^2-\frac{3}{2c^2}\vec{u}^2\right], \tag{2.4a}$$

$$g_i^{(eq)} = \begin{cases} w_i\rho e\left[-1.5\frac{u^2}{c^2}\right], & i=0, \\ w_i\rho e\left[1.5+\frac{1.5}{c^2}(\vec{e}_i\vec{u})+\frac{9}{2c^4}(\vec{e}_i\vec{u})^2-\frac{3}{2c^2}\vec{u}^2\right], & i=1,2,3,4, \\ w_i\rho e\left[3+\frac{6}{c^2}(\vec{e}_i\vec{u})+\frac{9}{2c^4}(\vec{e}_i\vec{u})^2-\frac{3}{2c^2}\vec{u}^2\right], & i=5,6,7,8. \end{cases} \tag{2.4b}$$

The discrete force ($F_i(\vec{x},t)$) and energy source ($Q_i(\vec{x},t)$) distribution functions can be written as:

$$F_i(\vec{x},t) = \left(1-\frac{1}{2\tau_f}\right)w_i\left[3\frac{\vec{e}_i-\vec{u}(\vec{x},t)}{c^2}+9\frac{\vec{e}_i\vec{u}(\vec{x},t)}{c^4}\vec{e}_i\right]\vec{F}(\vec{x},t), \tag{2.5a}$$

$$Q_i(\vec{x},t) = \left(1-\frac{1}{2\tau_g}\right)w_i Q(\vec{x},t), \tag{2.5b}$$

where $\vec{F}$ and Q are the force density and the energy source density term, respectively. The macroscopic density (ρ), velocity ($\vec{u}$), and internal energy per unit mass (e), are computed via the following equations [23, 35]:

$$\rho = \sum_i f_i = \sum_i f_i^{(eq)}, \tag{2.6a}$$

$$\rho\vec{u} = \sum_i \vec{e}_i f_i + \frac{\Delta t}{2}\vec{F}, \tag{2.6b}$$

$$\rho e = \sum_i g_i + \frac{\Delta t}{2}\vec{Q}. \tag{2.6c}$$

In the Lattice Boltzmann method, the relation between the mesoscopic evolution equation and the macroscopic conservation equations is derived by utilizing the Chapman-Enskog expansion [47]. This way, the kinematic viscosity (ν) and thermal diffusivity (α) read as follows:

$$\nu = \frac{1}{3}\left(\tau_f-\frac{1}{2}\right)c^2\Delta t, \tag{2.7a}$$

$$\alpha = \frac{2}{3}\left(\tau_g-\frac{1}{2}\right)c^2\Delta t. \tag{2.7b}$$

Eqs. (2.7a) and (2.7b) are used for calculating the relaxation times related to the LBE and TLBE. In the current study, the split-forcing LBE proposed by Guo et al. [44] is used to solve the fluid flow in presence of a stationary obstacle. Regarding to the advantage of this method, the same approach is considered for the TLBE of energy equation, too. In the actual calculation, the following four steps can be assumed for the split forcing TLBE:

https://doi.org/10.4208/cicp.060414.220115a Published online by Cambridge University Press

Step 1: First Forcing

$$\rho(\vec{x},t)\vec{u}(\vec{x},t)=\sum_i \vec{e}_i f_i(\vec{x},t)+\frac{\Delta t}{2}\vec{F}(\vec{x},t), \tag{2.8a}$$

$$e(\vec{x},t)=\sum_i g_i(\vec{x},t)+\frac{\Delta t}{2}\vec{Q}(\vec{x},t). \tag{2.8b}$$

Step 2: Collision

$$f_i'(\vec{x},t)=f_i(\vec{x},t)-\frac{1}{\tau_f}\left[f_i(\vec{x},t)-f_i^{(eq)}(\vec{x},t)\right], \tag{2.9a}$$

$$g_i'(\vec{x},t)=g_i(\vec{x},t)-\frac{1}{\tau_g}\left[g_i(\vec{x},t)-g_i^{(eq)}(\vec{x},t)\right]. \tag{2.9b}$$

Step 3: Second Forcing

$$f_i''(\vec{x},t)=f_i'(\vec{x},t)+\Delta t F_i(\vec{x},t), \tag{2.10a}$$

$$g_i''(\vec{x},t)=g_i'(\vec{x},t)+\Delta t Q_i(\vec{x},t). \tag{2.10b}$$

Step 4: Streaming

$$f_i(\vec{x}+e_i\Delta t,t+\Delta t)=f_i''(\vec{x},t), \tag{2.11a}$$

$$g_i(\vec{x}+e_i\Delta t,t+\Delta t)=g_i''(\vec{x},t), \tag{2.11b}$$

where f_i' and f_i'' are named post-collision and post-forcing particle density distribution functions, respectively [23]. Similarly, g_i' and g_i'' can be introduced as post-collision and post-forcing particle energy distribution functions, respectively.

2.2 The lattice Boltzmann method for non-Newtonian fluids

Unlike Newtonian fluids, whose viscosity is constant at all rates of shear; non-Newtonian fluids exhibit a non-linear relationship between the shear stress and the strain rate. Here, the power-law model is employed for describing the non-Newtonian characteristics of flows. The simple non-Newtonian power-law model is capable to describe both the shear-thinning and shear-thickening behaviors over moderate ranges of shear rates [8–11]. The rheological relationship of the power-law model is as follows [48]:

$$\nu=m(\dot{\gamma})^{n-1}, \tag{2.12}$$

where m and n are the consistency index and non-Newtonian behavior index, respectively. Considering $n<1$, the increase of stain rate causes the reduction of viscosity (pseudoplastic or shear-thinning fluid). Conversely, when $n>1$, the increase of stain rate causes the growth of viscosity (dilatant or shear-thickening fluid). Newtonian fluid is correspond to the case which $n=1$ and $m=\nu_0$. In the shear rate-dependent viscosity

https://doi.org/10.4208/cicp.060414.220115a Published online by Cambridge University Press

fluids, the shear rate ($\dot{\gamma}$) can be calculated from the second invariant of the rate-of-strain tensor as [49]:

$$\dot{\gamma}=2\sqrt{D_{ll}}, \tag{2.13}$$

where

$$D_{ll}=\sum_{\alpha,\beta=1}^{2} S_{\alpha\beta}S_{\alpha\beta}. \tag{2.14}$$

Eq. (2.14) must be evaluated at each point of fluid flow. In the common lattice Boltzmann approaches, the strain rate tensor can be evaluated macroscopically [50]:

$$S_{\alpha\beta}=\frac{1}{2}\left(\nabla_\beta u_\alpha+\nabla_\alpha u_\beta\right), \tag{2.15}$$

or locally in mesoscopic scale [51]:

$$S_{\alpha\beta}=-\left(1-\frac{1}{\tau}\right)\frac{1}{2\rho\nu}\sum_{i=1}^{9} c_{i\alpha}c_{i\beta}f_i^{(1)}. \tag{2.16}$$

2.3 Direct-forcing method

In this study, the direct-forcing method has been employed to calculate the effects of heated immersed boundary on fluid flow and temperature domains. The desired velocity must satisfy the no-slip condition on the boundary. The direct forcing formula in the LBE can be directly obtained as [23]:

$$\vec{F}(\vec{x},t+\Delta t)=2\rho(\vec{x},t+\Delta t)\frac{\vec{U}^d-\vec{u}^{noF}(\vec{x},t+\Delta t)}{\Delta t}, \tag{2.17}$$

where U^d and $u^{noF}(\vec{x},t+\Delta t)$ are the desired boundary velocity and the unforced velocity at the forcing point, respectively. Similarly, a direct forcing formula for boundary energy-forcing term can be derived [35]:

$$Q(\vec{x},t+\Delta t)=2\rho(\vec{x},t+\Delta t)\frac{c^2}{3T_0}\frac{T^d-T^{noE}(\vec{x},t+\Delta t)}{\Delta t}, \tag{2.18}$$

where T^d and $T^{noE}(\vec{x},t+\Delta t)$ are the desired temperature of the immersed boundary and the temperature under no external energy source at $(\vec{x},t+\Delta t)$, respectively.

3 Interface schemes

In the immersed boundary formulation, the on-lattice variables are located on the fixed Cartesian mesh, and the off-lattice variables are placed on the curvilinear mesh, without being constrained to adapt to the fixed Cartesian mesh [15]. Therefore, an additional interface scheme is required to link the off and on-lattice nodes. In this section, the interface schemes are subdivided into sharp and diffuse interface schemes.

https://doi.org/10.4208/cicp.060414.220115a Published online by Cambridge University Press

3.1 Sharp interface schemes

The sharp interface scheme was first proposed by Kim et al. [22], based on a finite-volume approach on a staggered mesh, together with a fractional-step method. This method was developed for lattice Boltzmann method by Kang and Hassan [23]. In the sharp interface scheme, forcing points (the points at which boundary forces are valued) are located on computational nodes neighboring to the immersed boundary. The interpolation technique is used for calculating the velocity (or temperature) on the forcing nodes. The interpolated values of velocity (or temperature) must satisfy the no-slip boundary condition (or desired thermal boundary condition). Table 1 shows the calculation steps for the IB-TLBM with sharp interface scheme. The method of interpolation scheme used in the sharp interface scheme has an important role on accuracy of solution.

Table 1: Sharp interface scheme's steps (between streaming and collision steps) [23].

(a)	Calculating unforced velocities of on-lattice nodes ($\vec{u}_{ij}^{noF}$). Calculating temperatures under no external energy source (T_{ij}^{noF}).
(b)	Update the velocities of on-lattice nodes by interpolating ($\vec{u}_{ij}$). Update the temperatures of on-lattice nodes by interpolating (T_{ij}).
(c)	Evaluating the boundary force on boundary points ($\vec{F}_{ij}=2\rho\frac{\vec{u}_{ij}-\vec{u}_{ij}^{noF}}{\Delta t}$). Evaluating the boundary energy-force on boundary points ($Q_{ij}=2\rho\frac{c^2}{3T_0}\frac{T_{ij}-T_{ij}^{noE}}{\Delta t}$).

Here, we used the interpolation method (with second order accuracy) proposed by Kim et al. [22]. These interpolations have been successfully validated by Kang and Hassan [23]. The schematic of the interpolation procedure is shown in Fig. 2. The aim of this interpolation is to satisfy the no-slip boundary conditions (or desired boundary's temperature) at the boundary point (red b point in Fig. 2) by calculating a suitable velocity (or temperature) on the forcing points (blue f point in Fig. 2). Regarding the available unforced fluid nodes, the following bilinear and linear interpolations are used for case 1 and case 2 (which are addressed in Fig. 2), respectively [23]:

$$\vec{u}_f=\frac{1}{\Delta_x\Delta_y}\left\{\vec{U}_b-\left[\Delta_x\left(1-\Delta_y\right)\vec{u}_2+\left(1-\Delta_x\right)\left(1-\Delta_y\right)\vec{u}_3+\Delta_y\left(1-\Delta_x\right)\vec{u}_4\right]\right\}, \tag{3.1a}$$

$$\begin{cases}\dfrac{1}{\Delta}\vec{U}_b-\dfrac{1-\Delta}{\Delta}\vec{u}_1 & \Delta\geqslant 0.5,\\ 2\vec{U}_b-2\Delta\vec{u}_1-(1-2\Delta)\vec{u}_2 & \Delta<0.5.\end{cases} \tag{3.1b}$$

https://doi.org/10.4208/cicp.060414.220115a Published online by Cambridge University Press

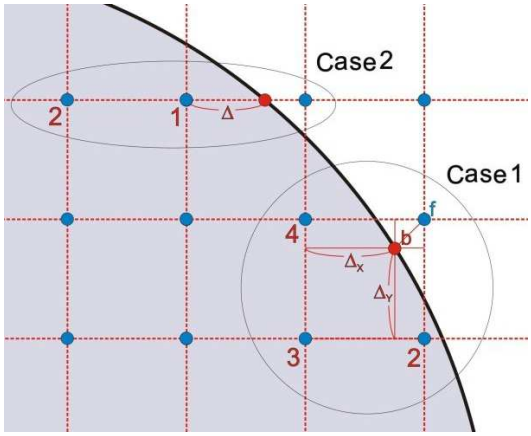


Figure 2: Schematic of sharp interface scheme [23].

3.2 Diffuse interface schemes

In the diffuse interface schemes, forcing points are placed on the surface of immersed boundary (off-lattice nodes) and the influence of the boundary force is distributed across adjacent computational (on-lattice) nodes (Fig. 3a). The reciprocal procedure is also needed for introducing the non-forced velocity (or temperature) from on-lattice nodes to corresponding off-lattice points (Fig. 3b). Table 2 shows the computational procedures of the diffuse interface schemes used here. It must be noticed that the updated velocity field, which is reconstructed via the boundary forces in step (e) of Table 2 does not guarantee the no-slip boundary condition on immersed boundary, because the forces used for updating the velocities are extracted from unforced velocities before updating. (step (c) in Table 2). To overcome this problem, the multi-direct-forcing method [52] is utilized.

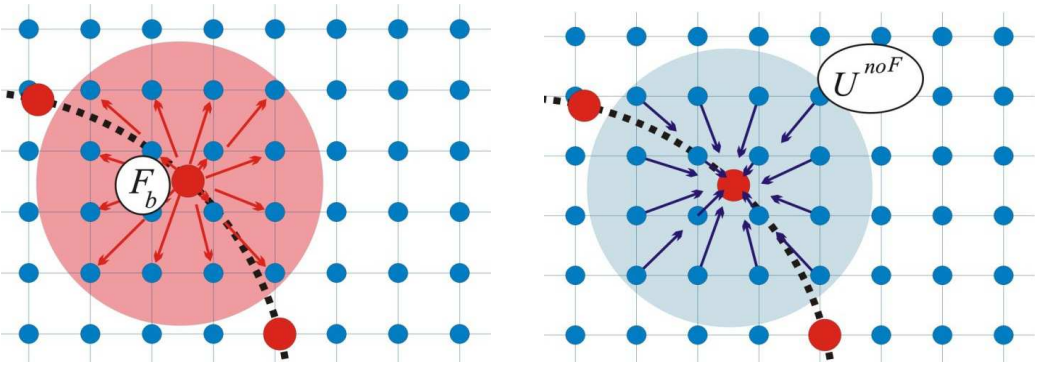


Figure 3: Schematic of velocity and force density exchanges between the on-lattice and off-lattice nodes: (a) the force densities, (b) unforced velocities [19].

https://doi.org/10.4208/cicp.060414.220115a Published online by Cambridge University Press

Table 2: Implicit diffuse interface scheme's steps (between streaming and collision steps) [23].

(a)	Calculating unforced velocities in on-lattice nodes ($\vec{u}_{ij}^{noF}$). Calculating temperatures under no external energy source (T_{ij}^{noE}).
(b)	Interpolating the unforced boundary velocities ($\vec{u}_b^{noF}=\sum_b \vec{u}_{ij}^{noF}\delta(x_{ij}-x_b)h^2$). Interpolating boundarys temperature under no external energy source ($T_b^{noE}=\sum_b T_{ij}^{noE}\delta(x_{ij}-x_b)h^2$).
(c)	Evaluating the boundary force on boundary point via the Eq. (2.17) ($\vec{F}_b$). Evaluating the boundary energy-force on boundary point via the Eq. (2.18) (Q_b).
(d)	Distributing the boundary force to neighboring on-lattice nodes ($\vec{F}_{ij}=\sum_b \vec{F}_b\delta(x_{ij}-x_b)\Delta s_b$). Distributing the boundary energy-force to neighboring on-lattice nodes ($Q_{ij}=\sum_b Q_b\delta(x_{ij}-x_b)\Delta s_b$).
(e)	Updating the velocities of neighboring on-lattice nodes (u_{ij}^F). Updating the temperatures of neighboring on-lattice nodes (T_{ij}^E).
(f)	Interpolating the forced boundary velocities ($\vec{u}_b^F=\sum_b \vec{u}_{ij}^F D(x_{ij}-x_b)h^2$). Interpolating energy-forced boundary temperature ($T_b^E=\sum_b T_{ij}^E\delta(x_{ij}-x_b)h^2$).
(g)	Iterating steps (c) to (f) until the desired criterion is satisfied.

As illustrated in Table 2, in the multi-direct-forcing method, the velocities of the boundary points are interpolated again with the new updated neighboring on-lattice nodes in the flow field. Then steps (c) to (f) are repeated until the desired accuracy is obtained. The number of these loops controls the degree of implicitness (NF) of the multi-direct-forcing method. Regarding to the steps (b), (d) and (f) of Table 2, a suitable discrete delta function (δ_h) must be utilized. Several discrete delta functions were introduced for this purpose [15, 23, 45, 46]. The discrete delta function includes a smoothed approximation to the Dirac delta function which is constructed according to certain principles. The vital postulates which are needed for extracting the acceptable interface function (δ_h) (that can be used in the interaction equation of immersed boundary methods) are described by Peskin [15]. According to Peskin's [15] investigation, δ_h in two-dimensions is given by the product of one-dimensional variable functions with mesh width (h):

$$\delta_h(\vec{x})=\frac{1}{h^2}\phi\left(\frac{x_1}{h}\right)\phi\left(\frac{x_2}{h}\right), \tag{3.2}$$

https://doi.org/10.4208/cicp.060414.220115a Published online by Cambridge University Press

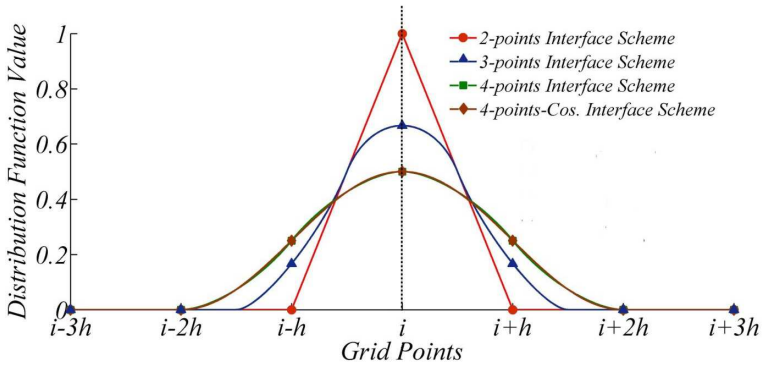


Figure 4: Values of distribution functions used for different interface schemes.

where x_1 and x_2 are the Cartesian component of $\vec{x}$. In the current study, four different types of diffuse interface schemes consisting of 2-points, 3-points, 4-points, and cosine type of 4- points (4-points-cos.) discrete approximations are employed:

- 2-points function [23]:

$$\phi(r)=\begin{cases} 1-|r|, & |r|\leqslant 1,\\ 0, & \text{otherwise,}\end{cases} \tag{3.3a}$$

- 3-points function [45]:

$$\phi(r)=\begin{cases} \frac{1}{6}\left(5-3|r|-\sqrt{-3(1-|r|)^2+1}\right), & 0.5\leqslant|r|<1.5,\\ \frac{1}{3}\left(1+\sqrt{-3r^2+1}\right), & |r|\leqslant 0.5,\\ 0, & \text{otherwise,}\end{cases} \tag{3.3b}$$

- 4-points function [15]:

$$\phi(r)=\begin{cases} \frac{1}{8}\left(3-2|r|+\sqrt{1+4|r|-4r^2}\right), & 0\leqslant|r|<1,\\ \frac{1}{8}\left(5-2|r|-\sqrt{-7+12|r|-4r^2}\right), & 1\leqslant|r|<2,\\ 0, & \text{otherwise,}\end{cases} \tag{3.3c}$$

- 4-points-cos. function [46]:

$$\phi(r)=\begin{cases} \frac{1}{4}\left(1+\cos\left(\frac{\pi r}{2}\right)\right), & |r|\leqslant 2,\\ 0, & \text{otherwise.}\end{cases} \tag{3.3d}$$

Fig. 4 shows the values of distribution functions near the boundary point. In this figure, the sharpness behavior of the aforementioned function is observable. Finally, before leaving this section, it is useful to emphasize the following points:

https://doi.org/10.4208/cicp.060414.220115a Published online by Cambridge University Press

Remark 3.1. It is desirable to narrow the support of δ_h for two reasons: first reducing computational cost, and second to improve the resolution of immersed boundary [15]. As shown in Fig. 3, only a restricted numbers of on-lattice nodes are involved by a specific boundary point.

Remark 3.2. The problem of an incomplete match of the no-slip boundary condition in diffuse interface schemes has also been pointed out by Shu et al. [53]. Wu and Shu [38] addressed this issue by introducing boundary condition-enforced IB-LBM. Boundary condition-enforced IB-LBM could perform as well as sharp IB-LBM.

Remark 3.3. Although the sharp interface method can satisfy exactly the no-slip boundary condition on immersed boundary, its implementation is significantly more laborious than the diffuse interface methods. This difficulty is due to the need of assessing whether the Eulerian node lies inside the immersed body or not.

4 Dimensionless parameters

In this section, the dimensionless parameters used in current study are defined and the methods of calculating surface forces and Nusselt numbers in IB-TLBM are discussed. The drag coefficient (C_D), and Strouhal number (St) are defined as follows:

$$C_D = \frac{F_D}{U_\infty^2 D/2}, \tag{4.1a}$$

$$St = \frac{f_q D}{U_\infty}, \tag{4.1b}$$

where f_q and D are the shedding frequency and diameter of the cylinder, respectively. The history of the drag coefficient is used to calculate the shedding frequency. In the case of stationary body, the surface force F_D can be calculated as the x-component of the following equation [23]:

$$\vec{F}_s = -\sum_b \vec{F}(\vec{x}_b)\Delta s_b = -\sum_{i,j} \vec{F}(\vec{x}_{ij})h^2, \tag{4.2}$$

where Δs_b is the arc length of immersed boundary. Both summations of Eq. (4.4) give the same results, but for the sharp interface scheme, only the second summation can be used.

Also, the following Reynolds number and Prandtl number for a power-law based flow are used in the current study:

$$\mathrm{Re} = \frac{U_\infty^{(2-n)} D^n}{m}, \tag{4.3a}$$

$$\mathrm{Pr} = \frac{m\rho c_p}{k}\left(\frac{U_\infty}{D}\right)^{(n-1)}, \tag{4.3b}$$

https://doi.org/10.4208/cicp.060414.220115a Published online by Cambridge University Press

where U_∞ represents the free stream velocity. For evaluation of Nusselt number, a new technique is introduced for current direct-forcing immersed boundary - thermal lattice Boltzmann method. This technique is developed based on the works of Wu et al. [40], Shu et al. [41], and Ren et al. [42, 43] for boundary condition-enforced IBM. The Nusselt number on the surface of boundary $(\vec{x}_b,t)$ is introduced as:

$$Nu(\vec{x}_b,t)=\frac{h(\vec{x}_b,t)\,L_c}{k}, \tag{4.4}$$

where L_c is characteristic length, h is convective heat transfer coefficient of the fluid and k is the thermal conductivity of the fluid and we have defined $k=\alpha\rho c_p$. By considering the energy balance at the surface of immersed boundary, we have:

$$h(\vec{x}_b,t)\,(T_b-T_\infty)=-k\frac{\partial T}{\partial n}(\vec{x}_b,t)=Q(\vec{x}_b,t), \tag{4.5}$$

where n is the normal direction to the immersed body in certain point of boundary. T_b and T_∞ are the temperature of boundary point and free stream, respectively. Comparing the equations (4.4) and (4.5) results in:

$$Nu_l(\vec{x}_b,t)=\frac{3T_0L_c}{\alpha\rho c^2\,(T_b-T_\infty)}Q(\vec{x}_b,t). \tag{4.6}$$

Also, the surface average Nusselt number can be obtained as follows:

$$Nu=\frac{3T_0L_c}{\alpha\rho c^2\,(T_b-T_\infty)\,L}\sum_l Q^l(\vec{x}_b,t)\,\Delta s_l. \tag{4.7}$$

Using Eqs. (4.6) and (4.7), the local and surface average Nusselt number can be achieved simply by predetermined parameters of direct-forcing IB-TLBM method. As it is seen form these equations, the solution processes does not include any difficult calculation of normal temperature gradient on immersed body surface which can significantly increase the speed of solution. This technique can be applied for each desired boundary curve in steady or unsteady flow regimes.

5 Results and discussion

In this section, the effects of various interface schemes of immersed boundary – thermal lattice Boltzmann method on the two-dimensional steady and unsteady non-Newtonian flow and heat transfer characteristics are studied. The power-law index lies in the range of $0.6<n<1.4$ thereby including both shear-thinning ($n<1$) and shear-thickening ($n>1$) non-Newtonian fluid behavior.

Similar to the work of Wu and Shu [40], the computational domain is taken as 60D$\times$ 40D and 50D$\times$40D uniform grid points for steady and unsteady flows, respectively. The

https://doi.org/10.4208/cicp.060414.220115a Published online by Cambridge University Press

Table 3: Grid independence study for steady (Re=40), and unsteady (Re=80) Newtonian fluid flow at Pr=0.7.

	Mesh grid	Number of on-lattice nodes (Nx×Ny)	Number of off-lattice points	Average drag coefficient	Average Nusselt number
Re=40	M1	600×400	47	1.467553	3.220490
	M2	1200×800	94	1.519606	3.275917
	M3	1800×1200	141	1.535271	3.270072
	M4	2400×1600	188	1.546021	3.276685
Re=80	M1	1000×800	94	1.29028	NAN
	M2	1500×1200	141	1.35777	4.56484
	M3	2000×1600	188	1.38191	4.56390
	M4	2500×2000	235	1.39584	4.59717

circular cylinder is placed at (20D, 20D). The mesh grid size of on-lattice nodes and number of off-lattice points have strong influence on consistency and accuracy of the numerical results. Optimal values of these parameters should be sufficiently fine to satisfactorily capture the flow and temperature fields, without overtaxing computational resources. In Table 3, the grid independence study (for both on-lattice and off-lattice) is carried out for steady (Re=40) and unsteady (Re 80) fluid flows, using the introduced IB-TLBM. It can be seen that, by changing the grid size from M3 to M4, the hydrodynamic and heat transfer results experience only minor variations (less than 1%) whereas a massive increase in the computational time has occurred. As a result, the mesh grid M3 is chosen to capture the flow and heat transfer phenomena in the current study. The boundary forcing points are uniformly distributed on the cylinder boundary with a spacing of $\Delta sb = h/1.5$.

5.1 Validation

As the energy equation is solved concurrently with the momentum equation, it seems that the validation of the obtained Nusselt number values provides a reasonable criterion for verification of the current numerical method. A comparison of heat transfer from cylinder to the Newtonian, shear-thinning and shear-thickening non-Newtonian fluids is presented in Table 4. In the cases of diffuse interface schemes, the implicitness is chosen to be NF=20. As it is reported in Table 4, the present results for all interface schemes are in close agreement with the previous methods presented in Table 2. It should be noted that the numerical results for non-Newtonian fluids are less accurate than the Newtonian fluids. This problem may be related to the non-linear viscous terms. In other words, different results with small variations may be obtained by different solvers or different grid sizes, as mentioned in literature [8, 9]. It seems that, due to the kinetic nature and local viscosity assessment of IB-TLBM, the results of this method can be considered as an assessment criterion for future works.

https://doi.org/10.4208/cicp.060414.220115a Published online by Cambridge University Press

Table 4: Comparison of the average Nusselt number (Nu) for heat transfer in power-law non-Newtonian fluids (Pr=1) from an unconfined circular cylinder at Re=40.

The characteristics of method	Year	$n=0.6$	$n=0.8$	$n=1.0$	$n=1.4$
Finite difference method [11]	2005	—	3.7359	3.5695	3.3249
Finite volume method, FLUENT. [9]	2007	—	3.9915	3.7030	3.3522
Finite volume method, FLUENT. [8]	2008	4.0545	3.8296	3.6533	3.4003
Finite volume method, FLUENT. [10]	2010	4.0775	—	3.6755	3.4216
Implicit diffuse direct-forcing (2-points), LBE	present	4.051846	3.869223	3.710647	3.467057
Implicit diffuse direct-forcing (3-points), LBE	present	4.074436	3.87648	3.712625	3.453490
Implicit diffuse direct-forcing (4-points), LBE	present	4.063633	3.869972	3.709672	3.461448
Implicit diffuse direct-forcing (4-Cos-points), LBE	present	4.06665	3.87365	3.713893	3.467948
Exterior sharp direct forcing, LBE	present	4.13382	3.8847	3.68549	3.394119

5.2 Comparison of numerical parameters

To find the accuracy of the method in satisfying the no-slip boundary condition and determined temperature on the immersed boundary, the following "hydrodynamic boundary error" (H.B.E) and "thermal boundary error" (T.B.E) are defined:

$$\text{H.B.E.}=\sqrt{\frac{1}{N_{ij}}\sum_i\sum_j\left(\vec{u}_b^{\,n}(i,j)-\vec{u}_b^{\,e}(i,j)\right)^2},$$
$$\text{T.B.E.}=\sqrt{\frac{1}{N_{ij}}\sum_i\sum_j\left(\vec{T}_b^{\,n}(i,j)-\vec{T}_b^{\,e}(i,j)\right)^2}, \tag{5.1}$$

where the superscript e and n refer to the exact value and the numerical result, respectively. In the case of stationary body $\vec{u}_b^{\,e}=0$. N_{ij} is the number of off-lattice nodes. The values of H.B.E and T.B.E for different types of interface scheme are presented in Figs. 5a and 5b, respectively. These figures are depicted in different power-law indices which covering Newtonian, shear thinning and shear thickening fluids. According to Fig. 5, both H.B.E and T.B.E decrease by increasing the power-law indices for all types of interface schemes. In other words, increasing the shear-thinning behavior leads to larger boundary errors using the IB-TLBM method. Inversely, the enhancement of shear-thickening results in more accurate solutions. According to Fig. 5b, the values of thermal boundary error increase by increasing of boundary sharpness. However, the 4-points-cos. interface scheme shows a different behavior for hydrodynamic boundary error. As seen from Fig. 5a, the 4-points, 3-points, 4-points-cos. and 2-points exhibit smaller hydrodynamic boundary errors, respectively. According to the Fig. 5a, in spite of using more interpolation points, the common 4-points-cos. interface does not provide more accurate results.

Fig. 6 shows the required number of iterations for satisfying convergence criterion i.e. $|CD^{(n+1)}-CD^{(n)}|<0.005$. Regarding the Fig. 6, the convergence time is increased by moving from shear-thinning to shear-thickening power-law fluid. Unlike the Newtonian

https://doi.org/10.4208/cicp.060414.220115a Published online by Cambridge University Press

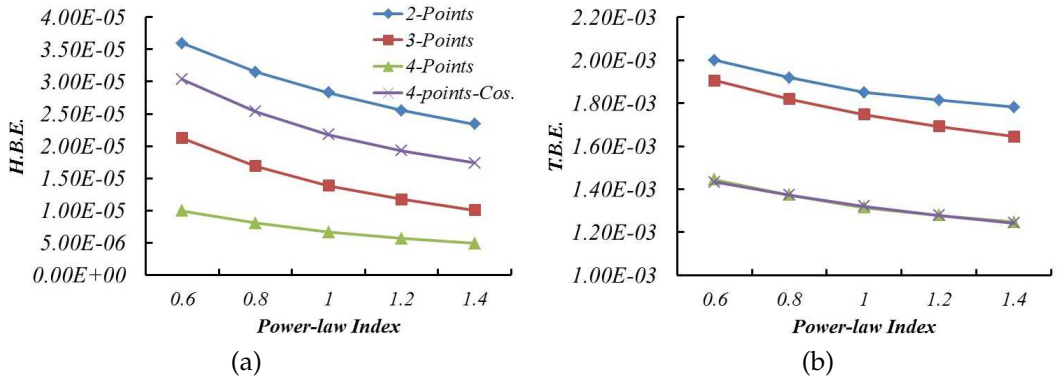


Figure 5: Values of (a) hydrodynamic and (b) thermal boundary errors respect to the power-law index for different interface schemes at Re=20.

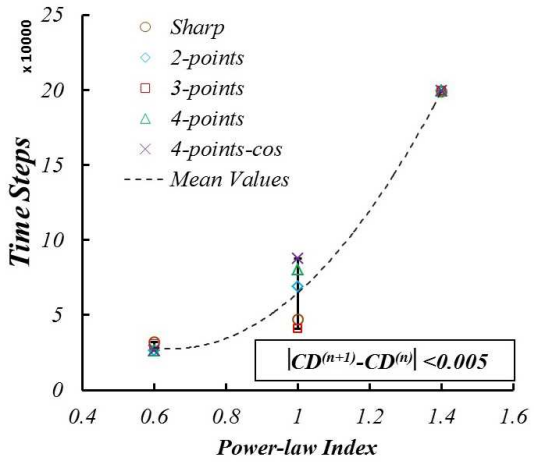


Figure 6: Number of iteration needed for convergence in shear-thinning, Newtonian and shear thickening fluids for different interface schemes at Re=20.

case, the required time steps for non-Newtonian power-law fluids are approximately the same for all the interface schemes.

Fig. 7 reports the values of CPU time taken to achieve the convergence criterion at $n=1.4$. As it is shown in Fig. 6, the time steps needed for convergence are almost the same for all interface schemes with $n=1.4$ (200000 iterations). Fig. 7 is depicted for both steady (Re=40) and unsteady (Re=80) cases. The mesh grid sizes presented in Table 3 is considered for steady and unsteady cases. Regarding Fig. 7, the sharp interface scheme is much faster than the diffuse interface schemes with a large numbers of grid points. Among the diffuse interface schemes, the 2-Points and 4-Points interfaces are the most and least efficient methods in terms of time complexity, respectively. The speed of the diffuse interface schemes reflects the number of interpolation points which are utilized (see Fig. 3). It is obvious that the computational cost increases with the size of the affected

https://doi.org/10.4208/cicp.060414.220115a Published online by Cambridge University Press

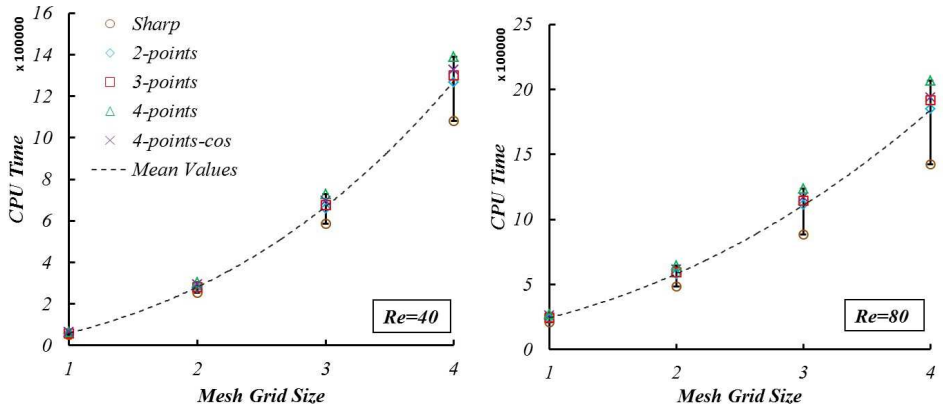


Figure 7: Values of CPU time needed for convergence of solution respect to mesh grid size in steady and unsteady flows for different interface schemes ($n=1.4$).

region (especially for multi-direct-forcing IB-TLBM). Therefore, the sharp and 4-points schemes are the best and worst methods, respectively.

5.3 Comparison of hydrodynamic parameters

Fig. 8 shows the dependence of the recirculation length on the power-law index for all the interface schemes. At the same value of the Reynolds number, the wake tends to be shorter in the shear-thinning fluids with respect to Newtonian and shear-thickening fluids. Because of the maximum rate of fluid deformation near the surface of immersed body, the viscosity is minimal in this region for shear-thinning fluids and a thin film of low viscosity fluid encapsulates the cylinder. With distance from the cylinder's boundary, the shear rate reduces to reach the higher viscosity of the fluid. The latter acts like

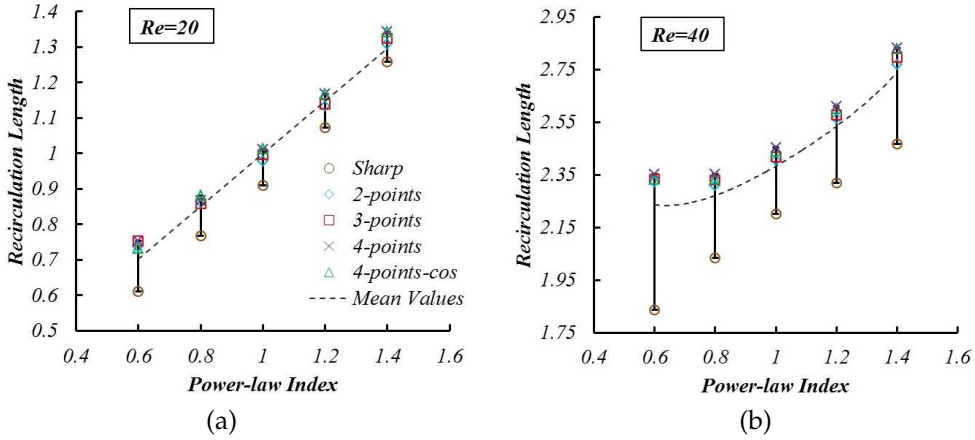


Figure 8: Values of recirculation length respect to the power-law index in steady flows for different interface schemes.

https://doi.org/10.4208/cicp.060414.220115a Published online by Cambridge University Press

an effective solid boundary which suppresses the tendency towards flow separation, so that separation is slightly delayed in shear-thinning fluids [16]. For the shear-thickening fluids, the high shear rate in the vicinity of the cylinder leads to high viscosity near the surface, and the slow moving viscous fluid encapsulates the cylinder. This slow moving viscous fluid meets the low viscosity fluids away from the cylinder. Therefore, in this case, the effective size of the bluff body increases leading to a higher value of the Reynolds number than its nominal value resulting in an earlier flow separation [16]. This tendency can be captured by all mentioned interface schemes for Re=20 (see Fig. 8a); for higher Reynolds number (see Fig. 8b), the prediction of diffuse interface schemes is inaccurate for shear-thinning fluids. In fact, this case shows a decrease of recirculation length when moving from shear-thinning into Newtonian behavior. The sharp interface scheme can capture the aforementioned tendency exactly for both Reynolds numbers. Although the values of L_w achieved by sharp method is noticeably lower than the corresponding values of the other methods, they lie nonetheless in acceptable range in comparison with the previous studies [23, 38].

The hydrodynamic drag force exerted by the fluid on the solid cylinder is composed of skin friction drag caused by shear stress on the surface of immersed body and the pressure drag due to the flow separation can be expressed in terms of dimensionless drag coefficient. Fig. 9 shows the variation of the drag coefficient with respect to the power-law index for different Reynolds numbers. Fig. 9 reports results for all diffuse and sharp interface schemes. As shown in Fig. 9, the drag coefficient generally increases as the power-law index increases for steady (Re= 20, 40) and unsteady (Re= 60, 80) fluid flows. This trend can be captured by the previous mentioned interface schemes. The sharp interface scheme experiences the smallest values of drag coefficient in comparison with other interface schemes. The amount of drag coefficient is a function of boundary sharpness. Generally, by decreasing the sharpness of immersed boundary from Sharp to 4-points interface schemes, the drag coefficient is increased. These changes are more pronounced in shear-thickening and higher Reynolds numbers. In addition, for accurate comparison, the values of drag coefficient in different power-law indices under the steady (Re=20, 40) and unsteady (Re=60, 80) flow regimes are presented in Tables 4 and 5, respectively.

Table 5: Drag coefficient for non-Newtonian power-law flow over an unconfined cylinder using different interface methods (steady cases Re=20, Re=40).

Interface Method	$n=0.6$		$n=0.8$		$n=1.0$		$n=1.2$		$n=1.4$	
	Re=20	Re=40	Re=20	Re=40	Re=20	Re=40	Re=20	Re=40	Re=20	Re=40
2-Points	1.799	1.232	1.950	1.400	2.075	1.537	2.173	1.652	2.258	1.749
3-Points	1.876	1.331	1.999	1.454	2.110	1.572	2.201	1.676	2.285	1.779
4-Points	1.883	1.333	2.006	1.458	2.117	1.576	2.208	1.681	2.287	1.778
4-Cos-Points	1.886	1.340	2.009	1.461	2.119	1.579	2.209	1.682	2.288	1.783
Sharp	1.799	1.232	1.950	1.400	2.075	1.537	2.173	1.652	2.258	1.749

https://doi.org/10.4208/cicp.060414.220115a Published online by Cambridge University Press

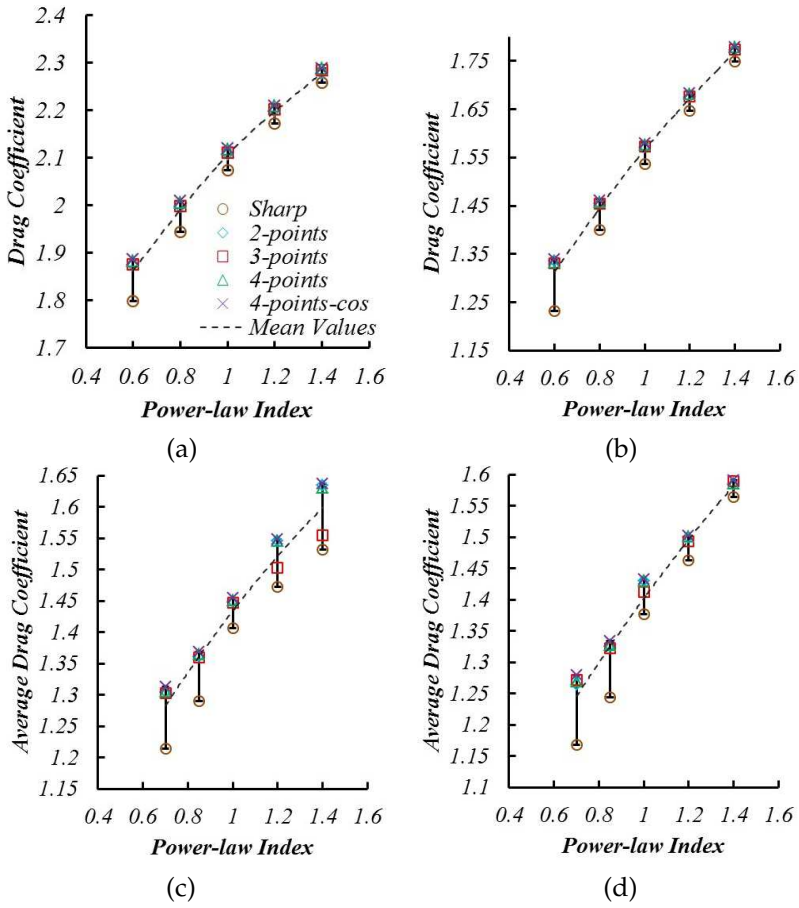


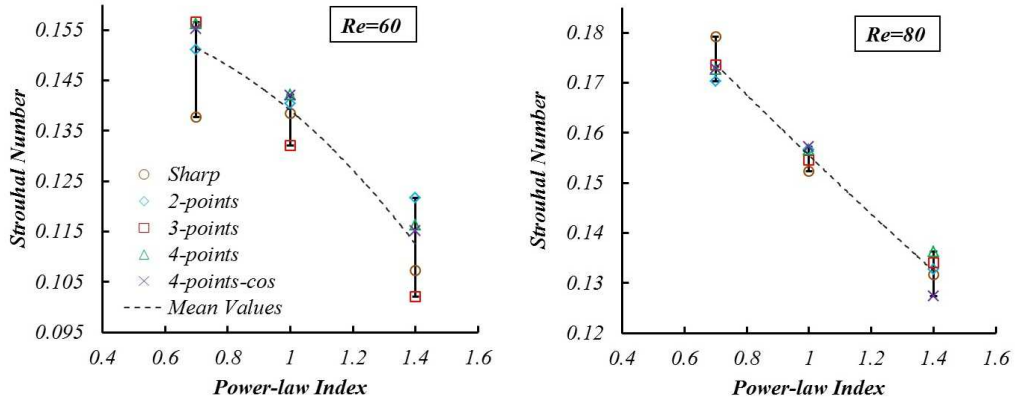
Figure 9: Values of (average) drag coefficient respect to the power-law index for different interface schemes and Reynolds numbers where (a) Re=20, (b) Re=40, (c) Re=60, (d) Re=80.

In the case of unsteady flows, Strouhal number is another applicable dimensionless number. Figs. 10a and 10b shows the values of Strouhal number with respect to the power-law index at Re= 60 and Re= 80, respectively. Regarding to the mean values of Fig. 10, Strouhal number will decrease when moving from shear-thinning to Newtonian and then shear-thickening fluids generally. The only exception is sharp interface method at Re=60.

5.4 Comparison of heat transfer parameter

In this section, the variation of the average Nusselt number with the power-law behavior index (n) and Reynolds number (Re) is considered as a criterion to compare thermal behavior of different interface schemes. Fig. 11 and Tables 6 and 7 illustrate the effects of power-law index and the Reynolds number on the averaged Nusselt number for sharp and diffuse interface schemes at Pr=1. Generally speaking, the average Nusselt number

https://doi.org/10.4208/cicp.060414.220115a Published online by Cambridge University Press



(a) (b)

Figure 10: Values of Strouhal number respect to the power-law index in unsteady flows for different interface schemes.

Table 6: Average drag coefficient for non-Newtonian power-law flow over an unconfined cylinder using different interface methods (unsteady cases Re=60, Re=80).

Interface Method	$n=0.7$		$n=0.85$		$n=1.0$		$n=1.2$		$n=1.4$	
	Re=60	Re=80	Re=60	Re=80	Re=60	Re=80	Re=60	Re=80	Re=60	Re=80
2-Points	1.304	1.275	1.361	1.325	1.449	1.431	1.546	1.500	1.634	1.585
3-Points	1.303	1.271	1.341	1.335	1.447	1.413	1.452	1.496	1.555	1.590
4-Points	1.306	1.269	1.365	1.328	1.444	1.430	1.546	1.501	1.630	1.586
4-Cos-Points	1.313	1.280	1.369	1.334	1.455	1.415	1.549	1.502	1.637	1.590
Sharp	1.214	1.168	1.248	1.262	1.407	1.377	1.428	1.466	1.533	1.564

Table 7: Average Nusselt number for heat transfer in non-Newtonian power-law flow (Pr=1) over an unconfined cylinder using different interface method (steady cases Re=20, Re=40).

Interface Method	$n=0.6$		$n=0.8$		$n=1.0$		$n=1.2$		$n=1.4$	
	Re=20	Re=40	Re=20	Re=40	Re=20	Re=40	Re=20	Re=40	Re=20	Re=40
2-Points	3.024	4.052	2.892	3.869	2.788	3.711	2.670	3.573	2.626	3.467
3-Points	3.034	4.074	2.899	3.876	2.790	3.713	2.697	3.567	2.623	3.449
4-Points	3.027	4.064	2.897	3.870	2.791	3.710	2.699	3.571	2.629	3.461
4-Cos-Points	3.028	4.067	2.898	3.874	2.794	3.714	2.703	3.576	2.633	3.460
Sharp	3.063	4.134	2.900	3.885	2.771	3.685	2.670	3.521	2.592	3.394

decreases with increasing shear-thinning ($n<1$) and decreases when the fluid behavior changes from Newtonian to shear-thickening characteristics for both steady (Re=20, 40) and unsteady (Re=60, 80) flow regimes. As a result, the shear-thickening ($n>1$) behavior

https://doi.org/10.4208/cicp.060414.220115a Published online by Cambridge University Press

Table 8: Average Nusselt number for heat transfer in non-Newtonian power-law flow (Pr=1) over an unconfined cylinder using different interface method (unsteady cases Re=60, Re=80).

Interface Method	$n=0.7$		$n=0.85$		$n=1.0$		$n=1.2$		$n=1.4$	
	Re=60	Re=80	Re=60	Re=80	Re=60	Re=80	Re=60	Re=80	Re=60	Re=80
2-Points	4.896	5.719	4.687	5.460	4.522	5.286	4.308	5.022	4.145	4.778
3-Points	4.908	5.730	4.649	5.403	4.445	5.183	4.223	4.992	4.054	4.743
4-Points	4.930	5.723	4.650	5.414	4.477	5.206	4.252	5.005	4.097	4.741
4-Cos-Points	4.886	5.717	4.724	5.471	4.526	5.245	4.269	5.026	4.166	4.834
Sharp	4.864	5.731	4.606	5.399	4.403	5.176	4.192	4.899	4.032	4.535

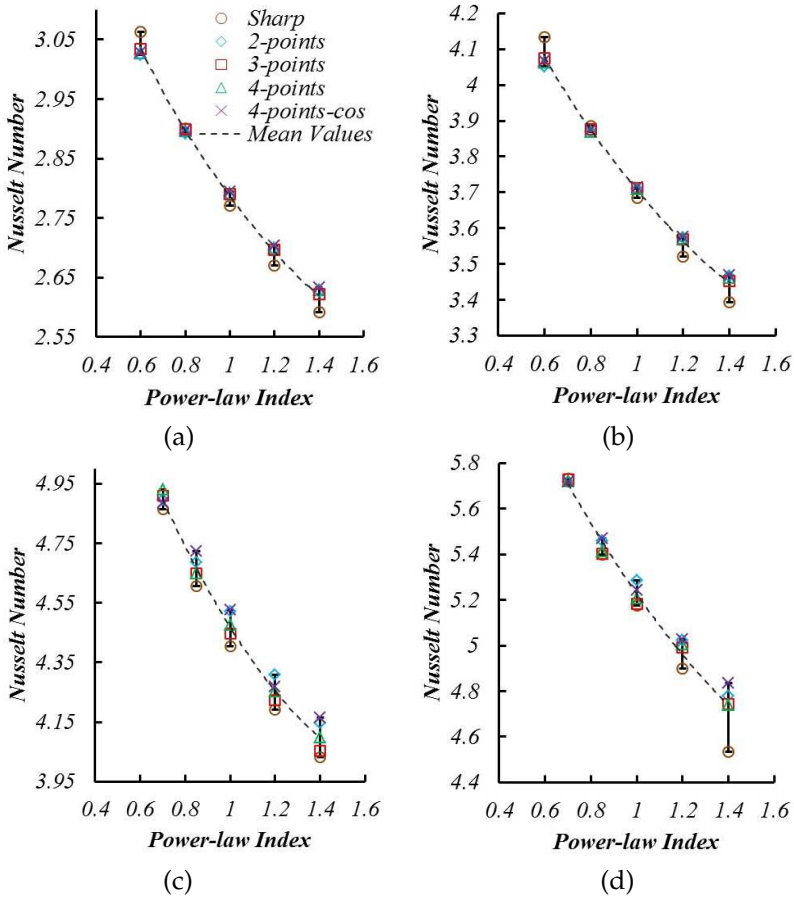


Figure 11: Values of average Nusselt number respect to the power-law index for different interface schemes and Reynolds numbers where (a) Re=20, (b) Re=40, (c) Re=60, (d) Re=80.

of fluid decreases heat transfer due to higher effective viscosity, and in contrast, the shear-thinning ($n<1$) fluids enhance the rate of heat transfer. This trend is apparent in the mean values reported for different interface schemes of IB-TLBM in Fig. 11. In comparison with

https://doi.org/10.4208/cicp.060414.220115a Published online by Cambridge University Press

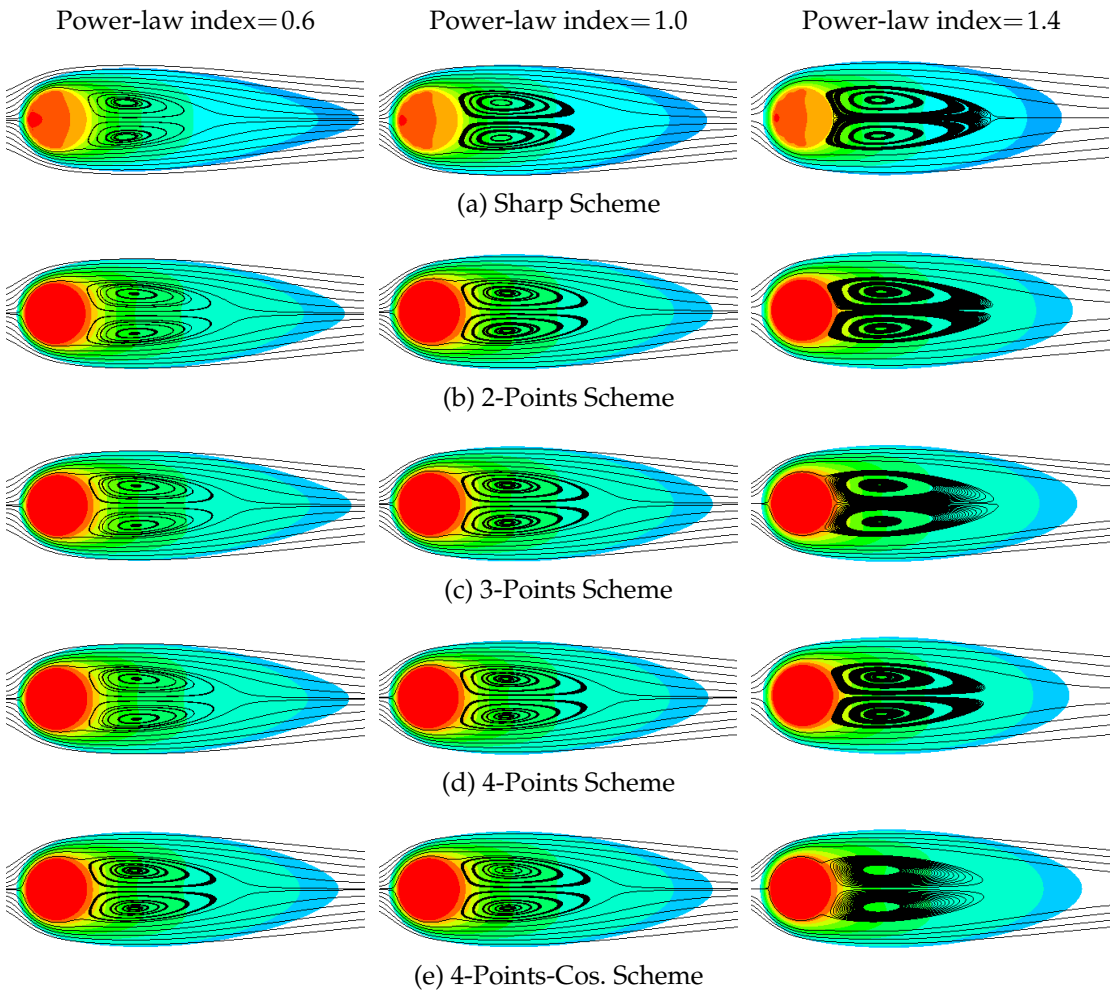


Figure 12: Streamline and isotherm contours for different power-law and interface schemes at Re=40.

the diffuse interface schemes, the sharp method shows smaller values in unsteady shear-thickening flows and higher values in the steady shear-thinning cases. Irrespective of the power-law fluid behavior, the average Nusselt number experiences increase trend by increasing the value of Reynolds number (for a given value of power-law index) for both Newtonian and non-Newtonian fluids at all interface schemes (refer to Tables 6 and 7). Both sharp and diffuse interface schemes show a good match with this trend.

Before closing the discussion, it is appropriate to visualize the configuration of the flow and temperature fields for different interface schemes. Streamlines and isotherm contours are usual representations for this purpose. Fig. 12 shows the representative plots of the streamlines and isotherms for different power-law indices and interface schemes. Regarding Fig. 12, as mentioned in previous sections, the wake length is obviously smaller

https://doi.org/10.4208/cicp.060414.220115a Published online by Cambridge University Press

for sharp interface scheme than diffuse interface schemes at all power-law indices. Also, the temperature contours show a deeper penetration of heat for sharp interface scheme, especially for shear-thinning fluid flows.

6 Conclusions

In this paper, the direct-forcing immersed boundary – thermal lattice Boltzmann method is introduced as an alternative technique for simulating flow and heat transfer in non-Newtonian fluids. The common benchmark of fluid flow over a stationary cylinder is considered as the test geometry. The results of the proposed IB-TLBM are validated against the existing finite volume and finite difference methods. Different variants of this method (with respect to the interface schemes) are investigated, to assess the most convenient interface scheme for predicting non-Newtonian fluid behavior. It the case of diffuse interface schemes, the 4-points algorithm appears to be the most accurate scheme for satisfying the hydrodynamic and thermal boundary conditions. Based on the obtained results for the recirculation length, the sharp interface scheme offers a better prediction of flow behavior in steady regimes. Finally, considering both criteria of accuracy and computational cost, the sharp interface scheme appears to be the preferred scheme for the current simulation. It must be noted, however, that the implementation of sharp interface scheme is significantly more laborious than the diffuse interface schemes. Regarding the advantage of immersed boundary methods, the current validated IB-TLBM model can be readily utilized for the simulation of moving heated bodies in non-Newtonian fluids.

References

[1] R. Clift, J. Grace, and M.E. Weber, Bubbles, Drops and Particles, Academic Press, New York, USA, 1978.
[2] M. Coutanceau, and J.-R. Defaye, Circular cylinder wake configuration: A flow visualization survey, Appl. Mech. Rev., 44 (1991), 255-305.
[3] C.H.K. Williamson, Vortex dynamics in the cylinder wake, Annu. Rev. Fluid Mech., 28 (1996), 477-539.
[4] C. Sasmal, and R.P. Chhabra, Laminar natural convection from a heated square cylinder immersed in power-law liquids, J. Non-Newtonian Fluid Mech., 166 (2011), 811-830.
[5] R.K. Gupta, Polymer and Composites Rheology, second ed., Marcel Dekker, New York, 2000.
[6] P. Sivakumar, R.P. Bharti, and R.P. Chhabra, Effect of power-lawindex on critical parameters for power-law flow across an unconfined circular cylinder, Chem. Eng. Sci., 61 (2006), 6035-6046.
[7] R.P. Chhabra, Bubbles, Drops and Particles in Non-Newtonian Fluids, second ed., CRC Press, Boca Raton, FL, 2006.
[8] R.P. Bharti, P. Sivakumar, and R.P. Chhabra, Forced convection heat transfer from an elliptical cylinder to power-law fluids, Int. J. Heat Mass Transfer, 51 (2008), 1838-1853.
[9] R.P. Bharti, R.P. Chhabra, and V. Eswaran, Steady forced convection heat transfer from a heated circular cylinder to power-law fluids, Int. J. Heat Mass Transfer, 50 (2007), 977-990.

https://doi.org/10.4208/cicp.060414.220115a Published online by Cambridge University Press

[10] V.K. Patnana, R.P. Bharti, and R.P. Chhabra, Two-dimensional unsteady forced convection heat transfer in power-law fluids from a cylinder, Int. J. Heat Mass Transfer, 53 (2010), 4152-4167.
[11] A. A. Soares, J. M. Ferreira, and R. P. Chhabra, Flow and Forced Convection Heat Transfer in Crossflow of Non-Newtonian Fluids over a Circular Cylinder, Ind. Eng. Chem. Res., 44 (2005), 5815-5827.
[12] C.S. Peskin, Flow patterns around heart valves: A digital computer method for solving the equations of motion, PhD thesis, Physiol, Albert Einstein Coll. Med., Univ. Microfilms, 378 (1972), 72-30.
[13] R. Verzicco, J. Mohd-Yusof, P. Orlandi, and D. Haworth, Large eddy simulation in complex geometric configurations using boundary body forces, AIAA J., 38 (2000), 427-433.
[14] E.A. Fadlun, R. Verzicco, P. Orlandi, and J. Mohd-Yusof, Combined immersed boundary finite difference methods for three dimensional complex flow simulations, J. Comput. Phys., 161 (2000), 35-60.
[15] C.S. Peskin, The immersed boundary method, Acta Numerica, 11 (2002), 479-517.
[16] A. Amiri Delouei, M. Nazari, M.H. Kayhani, and S. Succi, Non-Newtonian unconfined flow and heat transfer over a heated cylinder using the direct-forcing immersed boundary-thermal lattice Boltzmann method, Phys. Rev. E, 89 (2014), 053312.
[17] J. Mohd-Yusof, Combined immersed boundaries/B-spline methods for simulations of flows in complex geometries, CTR Annual Research Briefs, NASA Ames/Stanford University, (1997), 317-327.
[18] X.D. Niu, C. Shu, Y.T. Chew, and Y. Peng, A momentum exchange-based immersed boundary-lattice Boltzmann method for simulating incompressible viscous flows, Physics Letters A, 354 (2006), 173-182
[19] H.Z. Yuan, X.D. Niu, S. Shu, M. Li, and H. Yamaguchi, A momentum exchange-based immersed boundary-lattice Boltzmann method for simulating a flexible filament in an incompressible flow, Comput. Math. App., 67 (2014), 1039-1056.
[20] A.J.C. Ladd, Numerical simulations of particulate suspensions via a discretized Boltzmann equation. Part 1. Theoretical foundation, J. Fluid Mech., 271 (1994), 285-309.
[21] A.L.F.L.E. Silva, A. Silveira-Neto, and J.J.R. Damasceno, Numerical simulation of two-dimensional flows over a circular cylinder using the immersed boundary method, J. Comput. Phys., 189 (2003), 351-370.
[22] J. Kim, D. Kim, and H. Choi, An immersed-boundary finite-volume method for simulations of flow in complex geometries, J. Comput. phys., 171 (2001), 132-150.
[23] S.K. Kang, and Y.A. Hassan, A comparative study of direct-forcing immersed boundary-lattice Boltzmann methods for stationary complex boundaries, Int. J. Numer. Meth. Fluids, 66 (2011), 1132-1158.
[24] R. Benzi, S. Succi, and M. Vergassola, The lattice Boltzmann equation: Theory and applications, Phys. Rep., 222 (1992), 145-197.
[25] G. Pontrelli, S. Ubertini, and S. Succi, The unstructured lattice Boltzmann method for non-Newtonian flows, J. Stat. Mech.: Theory and Exp., (2009) P06005.
[26] S. Melchionna, M. Bernaschi, S. Succi, E. Kaxiras, F. J. Rybicki, D. Mitsouras, A. U. Coskun, and C.L. Feldman, Hydrokinetic approach to large-scale cardiovascular blood flow, Comput. Phys. Commun., 181 (2010), 462-472.
[27] A.D. Maio, S. Palpacelli, and S. Succi, A new boundary condition for three-dimensional lattice Boltzmann simulations of capillary filling in rough micro-channels. Commun. Comput. Phys., 9 (2011), 1284-1292.

https://doi.org/10.4208/cicp.060414.220115a Published online by Cambridge University Press

[28] T. Zhang, B. Shi, Z. Chai, and F. Rong, Lattice BGK model for incompressible axisymmetric flows, Commun. Comput. Phys., 11 (2012), 1569-1590.
[29] L. Wang, Z. Guo, B. Shi, and C. Zheng, Evaluation of three lattice Boltzmann models for particulate flows, Commun. Comput. Phys., 13 (2013), 1151-1172.
[30] A.M. Artoli, and A. Sequeira, Mesoscopic simulations of unsteady shear-thinning flows, in: Lecture Notes in Comput. Sci. Springer, Berlin, 3992 (2006), 78-85.
[31] S. Gabbanelli, G. Drazer, and J. Koplik, Lattice Boltzmann method for non-Newtonian (Power-Law) fluids, Phys. Rev. E., 72 (2005), 046312.
[32] R. Mei, L.S. Luo, and W. Shyy, An accurate curved boundary treatment in the lattice Boltzmann method, J. Comput. Phys., 155 (1999), 307-330.
[33] Z. Guo, C. Zheng, and B. Shi, An extrapolation method for boundary conditions in lattice Boltzmann method, Phys. Fluids, 14 (2002), 2007-2010.
[34] Y. Cheng, L. Zhu, and C. Zhang, Numerical study of stability and accuracy of the immersed boundary method coupled to the lattice Boltzmann BGK model, Commun. Comput. Phys., 16 (2014), 136-168.
[35] S.K. Kang, and Y.A. Hassan, A direct-forcing immersed boundary method for the thermal lattice Boltzmann method, Comput. Fluids, 49 (2011), 36-45.
[36] S.C. Fu, W.W.F. Leung, and R.M.C. So, A lattice Boltzmann and immersed boundary scheme for model blood flow in constricted pipes: Part 1 - Steady flow, Commun. Comput. Phys., 14 (2013), 126-152.
[37] S.C. Fu, R.M.C. So, and W.W.F. Leung, A lattice Boltzmann and immersed boundary scheme for model blood flow in constricted pipes: Part 2 - Pulsatile flow, Commun. Comput. Phys., 14 (2013), 153-173.
[38] J. Wu, and C. Shu, Implicit velocity correction-based immersed boundary-lattice Boltzmann method and its applications, J. Comput. Phys., 228 (2009), 1963-1979.
[39] J. Wu, and C. Shu, Particulate flow simulation via a boundary condition-enforced immersed boundary-lattice Boltzmann scheme, Commun. Comput. Phys., 7 (2010), 793-812.
[40] J. Wu, C. Shu, and N. Zhao, Simulation of thermal flow problems via a hybrid immersed boundary-lattice Boltzmann method, J. App. Math., Article ID 161484 (2012).
[41] C. Shu, W.W. Ren, and W.M. Yang, Novel immersed boundary methods for thermal flow problems, Int. J. Numer. Meth. Heat Fluid Flow, 23 (2013), 124-142.
[42] W.W. Ren, C. Shu, J. Wu, and W.M. Yang, Boundary condition-enforced immersed boundary method for thermal flow problems with Dirichlet temperature condition and its applications, Comput. Fluids, 57 (2012), 40-51.
[43] W.W. Ren, C. Shu, and W.M. Yang, An efficient immersed boundary method for thermal flow problems with heat flux boundary conditions, Int. J. Heat Mass Transfer, 64 (2013), 694-705.
[44] Z. Guo, C. Zheng, and B. Shi, Discrete lattice effects on the forcing term in the lattice Boltzmann method, Phys. Rev. E., 65 (2002), 046308.
[45] A.M. Roma, C.S. Peskin, and M.J. Berger, An Adaptive Version of the Immersed Boundary Method, J. Comput. Phys., 153 (1999), 509-534.
[46] C.S. Peskin, Numerical analysis of blood flow in the heart, J. Comput. Phys., 25 (1977), 220-252.
[47] B. Chopard, and M. Droz, Cellular Automata Modeling of Physical Systems, Cambridge University Press, Cambridge, UK, 1998.
[48] C.H. Wang, and J.R. Ho, A lattice Boltzmann approach for the non-Newtonian effect in the blood flow, Comput. Math. Appl., 62 (2011), 75-86.
[49] A. Nejat, V. Abdollahi, and K. Vahidkhah, Lattice Boltzmann simulation of non-Newtonian

https://doi.org/10.4208/cicp.060414.220115a Published online by Cambridge University Press

flows past confined cylinders, J. Non-Newtonian Fluid Mech., 166 (2011), 689-697.
[50] Z.G. Feng, and E.E. Michaelides, Proteus: A direct forcing method in the simulation of particulate flows, J. Comput. Phys., 202 (2005), 20-51.
[51] Y.Sui, Y.T. Chew, P. Roy, and H.T. Low, A hybrid immersed-boundary and multi-block lattice Boltzmann method for simulating fluid and moving-boundaries interactions, Int. J. Numer. Meth. Fluids, 53 (2007), 1727-1754.
[52] K. Luo, J. Wang, and K. Cen, Full-scale solutions to particle-laden flows: Multidirect forcing and immersed boundary method, Phys. Rev. E., 76 (2007), 066709.
[53] C. Shu, N. Liu, and Y.T. Chew, A novel immersed boundary velocity correction-lattice Boltzmann method and its application to simulate flow past a circular cylinder, J. Comput. Phys., 226 (2007), 1607-1622.

https://doi.org/10.4208/cicp.060414.220115a Published online by Cambridge University Press